Extending Proton Energy Gain in Laser Driven Helical Coil Targets

Contact: *sferguson25@qub.ac.uk

S. Ferguson*, B. Greenwood, B. Odlozilik, M. Alanazi, M. Borghesi & S. Kar
Centre for Plasma Physics, Queen's University Belfast, BT7 1NN, UK

E. Aktan & M. Cerchez
Institute for Laser and Plasma Physics, Heinrich Heine University of Düsseldorf, D-40225, Germany

D. Doria
Extreme Light Infrastructure - Nuclear Physics, Horia Hulubei National Institute, 077125, Romania

H. Ahmed & J. Green
Central Laser Facility, STFC Rutherford Appleton Laboratory, OX11 0QX, UK

Abstract

Laser driven helical coil targets post-accelerate and focus TNSA beams to from a quasi-collimated, narrow energy band of protons. Increasing the length of helical coil extends the duration protons remain in phase with the strong electric fields formed by the helical coil target. Therefore, longer helical coils are expected to enhance the acceleration and focussing effects which was observed in our recent experiment at Vulcan's target area west with helical coil length up to $\sim 12mm$. Particle tracing simulations closely resemble the experimental data and reveal that the helical coil effectiveness is significantly reduced after $\sim 12mm$. The reduced effectiveness is attributed to accelerated protons outrunning, thus dephasing with the strong electric field region produced by helical coils of fixed pitch and radius.

1 Introduction

The target normal sheath acceleration (TNSA) mechanism is currently the most robust method of generating ion beams with relativistically intense lasers [1]. Unfortunately TNSA ion beams are of wide divergence with a broadband energy spectrum making them unsuitable for applications such as hadrontherapy [2–5]. Consequently methods to increase energy and manipulate ions into focussed, collimated beams with mono-energetic features have attracted significant research interest.

One method proposed is the novel helical coil (HC) target in Kar *et al.* [9]. The method employs a helix of wire attached perpendicular to the rear of a standard $\sim 10s\ \mu m$ thick flat foil TNSA target. Under laser irradiation a TNSA beam is generated within the wire helix. Additionally, a positive unipolar EM pulse is formed by the laser irradiation and propagates along the wire helix towards ground neutralising the positively charged target foil [6–8]. The EM pulse typically spans a few turns of helix wire, thus forms an annular electric field structure around the proton beam which then co-propagate along the helix axis. The longitudinal electric field component accelerates protons along the helix axis while the radial field focusses protons towards the axis. The result is a quasi-collimated proton beam with a narrowband spectral peak due to focussing and energy gain of the protons in the helical coil target [9–13].

In order for HCs to be effective the synchronisation between the EM pulse and the given protons along the helix axis must be maintained [12, 13]. Therefore the proton time of flight must be equivalent to the EM pulse propagation time over one turn and,

$$\frac{p}{r} = 2\pi\sqrt{\frac{\beta_z^2}{\beta_{EM}^2 - \beta_z^2}} \tag{1}$$

where p is the pitch, r the radius with EM pulse speed along the wire $\beta_{EM} = v_{EM}/c$ and proton speed along the helix axis $\beta_z = v_z/c$ normalised to the speed of light. The proton speed is dependant on kinetic energy and for a desired energy, known as the synchronisation energy, a suitable ratio between HC pitch and diameter is estimated from equation 1.

HC target length is another important parameter that impacts operation. Consider two identical HCs differentiated only in length. The longer HC is constructed from an increased length of wire than the shorter prolonging the EM pulse travel time to the end of the HC. Therefore protons propagating synchronously along the helix axis with the EM field experience the focussing and accelerating fields for an increased duration in a longer HC. These protons which travel with the field for longer should experience greater energy gain and divergence reduction. To summarise, a longer HC should produce a lower divergence proton beam at a higher energy compared to a shorter HC.

2 Experiment

The helical coil (HC) experiment presented here was performed in Target Area West (TAW) of the Vulcan laser system at the Central Laser Facility. Vulcan's beam eight ($B8$) was employed to irradiate HC targets with energies up to $80J$ pre-compressor in a $(2.5 \pm 0.3)ps$ pulse

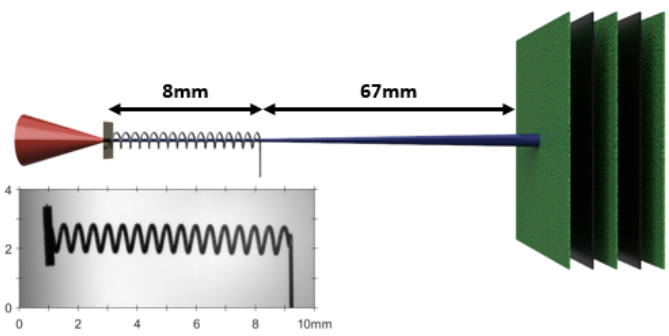

Figure 1: Experimental set up of a typical helical coil (HC) experiment. A laser (red) irradiates the foil section of the HC generating a seed proton beam (blue) within the HC that is focussed and accelerated by the helix section. The proton beam is detected by a RCF stack at a significant distance from the exit of the HC. HC length and HC to RCF distances included. Inset: calibrated photo of a experimentally deployed HC target.

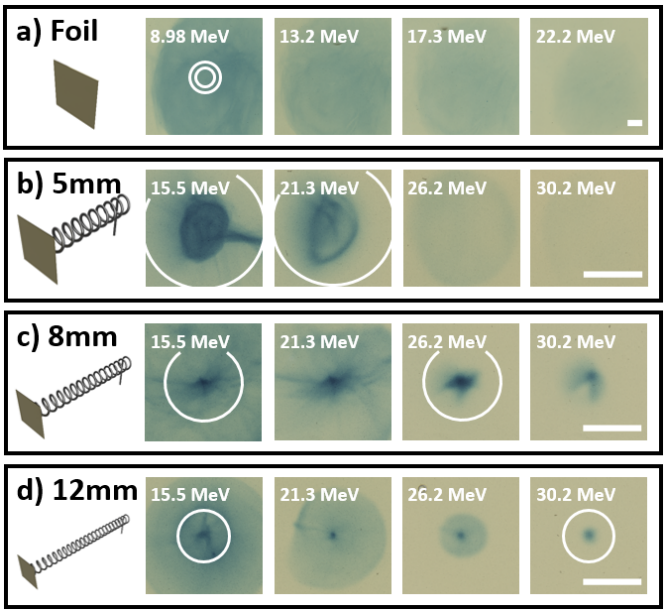

Figure 2: Proton beams observed on RCF for **(a)** reference flat foil, **(b)** $\sim 5mm$, **(c)** $\sim 8mm$ and **(d)** $\sim 12mm$ long helical coils (HC). HCs had $500\mu m$ pitch, $700\mu m$ inner diameter. RCF was deployed at $75mm$ from the proton source (laser-target interaction). RCF dimensions are (a) $40 \times 40mm$ and (b-d) $10 \times 10mm$ (scale bars are $5mm$). White circles represent the HC aperture with half-angle divergence (b) 4.0°, (c) 2.5° and (d) 1.7°. As a reference, 4.0° and 2.5° divergences are also shown in (a).

duration at a wavelength of $1053nm$. The laser focal spot was optimised to a $\sim 4\mu m$ FWHM on target with a $f/3$ parabola, irradiating HC targets with intensities $\sim 3 \times 10^{19} W/cm^2$.

The experimental set up is shown in figure 1. $B8$ (red) irradiates the HC target generating a TNSA seed proton beam (blue) within the HC that is focussed and accelerated by the helix section of the target. The proton beam is detected on a stack of radiochromtic film (RCF) deployed $75mm$ from the proton source (laser-target interaction). RCF is an ideal diagnostic due to its ability to simultaneously detect spatial and spectral profiles of the resultant proton beams [14–17].

HC targets were constructed from $125\mu m$ diameter stainless steel wire to have $700\mu m$ inner diameter and $500\mu m$ pitch with various lengths between $4 - 12mm$. For the purposes of calculations the HC diameter is measured from the wire centre thus $2r = (700+125)\mu m$. The laser was incident on a $2 \times 2mm$ square of $25\mu m$ thick Au foil attached perpendicular to the helix axis. The target was supported at the opposite end to the foil by a $125\mu m$ wire glued to a target stalk.

3 Results

The parameters of the EM pulse travelling along the helical coil (HC) wire are of paramount importance in understanding HC acceleration. These were measured following the method outlined by Ahmed *et al.* [7]. The EM pulse had a peak linear charge density $\lambda \simeq 23 \pm 3\mu C/m$ and an asymmetric gaussian profile with $t_r \simeq 6ps$ HWHM rise and $t_d \simeq 20ps$ HWHM decay times containing a total charge estimated $\sim 190nC$. The EM pulse parameters measured here are in broad agreement with references [6–13]. The EM pulse propagates at near the speed of light $\beta_{EM} \simeq 0.98c$ [7] traversing the entire wire length of one HC turn in approximately $9ps$. Therefore the strong electric field region spans ~ 3 turns of the HC target, the rise HWHM extending ~ 0.7 turns in front of the peak EM field and the decay HWHM ~ 2.3 turns behind.

To investigate the impact of length, HC targets with lengths measured $(4.74 \pm 0.04)mm$, $(8.02 \pm 0.04)mm$ and $(12.14 \pm 0.04)mm$ were deployed. The HCs share the same pitch and diameter hence the synchronisation energy should remain constant irrespective of the HC length. Equation 1 suggests a $16.6MeV$ synchronisation energy for the $(700+125)\mu m$ diameter and $500\mu m$ pitch HCs investigated here. Figure 2 presents a comparison of proton beams detected on RCF for the three lengths of HC alongside a flat foil reference representative of the TNSA seed proton beam within the HC targets. The seed beam observed has wide divergence $> 10°$ (half-angle) with a smooth beam profile up to a $27 \pm 3MeV$ maximum energy cut off (aggregated from several flat foil references not shown). In contrast the three various length HC proton beams exhibit focussed beams beyond the TNSA seed cut off energy.

The HC proton beams exhibit significant divergence

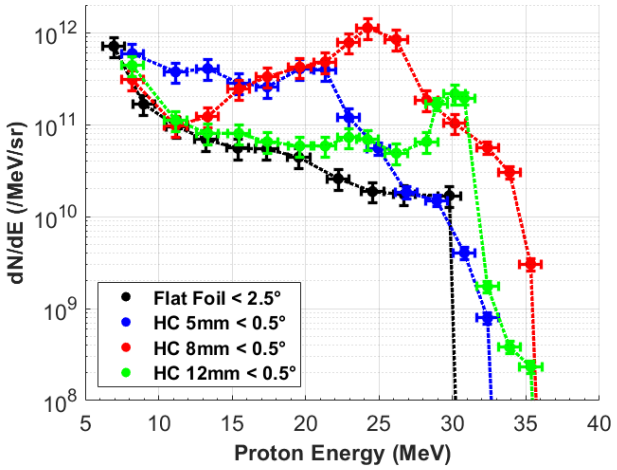

Figure 3: Spectra extracted from RCF for increasing length of helical coil (HC). HCs were $\sim 5mm$ (blue), $\sim 8mm$ (red) and $\sim 12mm$ (green) long. Spectral peaks are observed at $\sim 21MeV$, $\sim 25MeV$ and $\sim 30MeV$ for increasing HC length. Also shown is the spectra extracted from a flat foil reference (black) representative of the TNSA seed beam manipulated by HCs. HC spectra were extracted for their $< 0.5°$ half angle divergence focussed beams and $< 2.5°$ for the flat foil reference, the exit aperture of the $\sim 8mm$ HC.

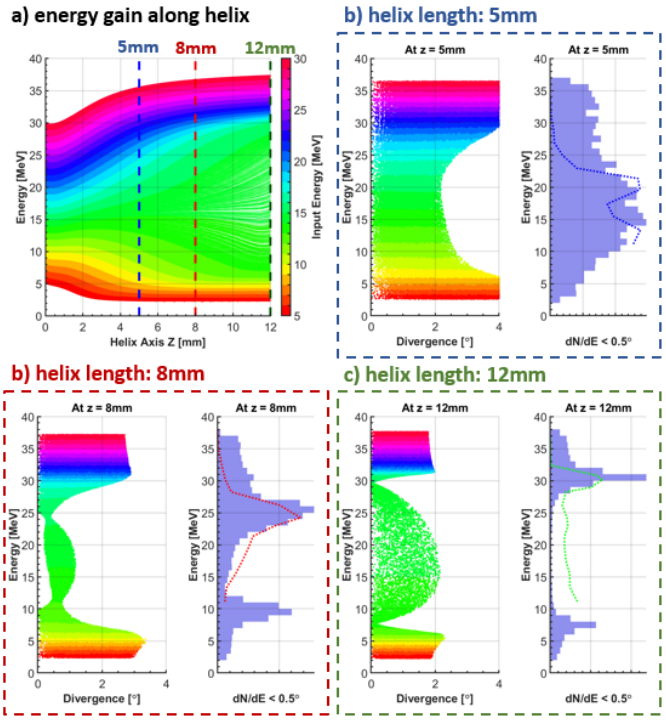

Figure 4: Particle tracing simulations performed in *PTRACE* for a helical coil (HC) of increasing length. **(a)** energy change along the helix axis. The simulated seed beam had $5 - 30MeV$ protons with $< 2.5°$ divergence where the colour scale corresponds to input proton energy. Divergence and spectral plots for a $< 0.5°$ output beam are extracted for HC length **(b)** $5mm$ (blue box), **(c)** $8mm$ (red box) and **(d)** $12mm$ (green box). Corresponding experimental spectra from figure 3 are over-plotted on simulation spectra as dotted lines.

reduction compared to their HC aperture half-angles; 4.0°, 2.5° and 1.7° (shown as white circles in figure 2). As expected divergence reduces with increasing HC length and the tightest beam focus observed for the $\sim 12mm$ long HC. The $\sim 5mm$ long HC exhibits an annular beam structure implying the HC is too short for effective focussing. Once dose converted, the tightest beam profiles for $\sim 5mm$, $\sim 8mm$ and $\sim 12mm$ long HCs are observed at $\sim 19.6MeV$, $\sim 26.2MeV$ and $\sim 30.8MeV$ respectively, with FWHM half-angle divergences $\sim 2.5°$, $\sim 0.5°$ and $\sim 0.3°$. The most significant reduction in focus FWHM occurs between $5mm$ and $8mm$ long HCs. Therefore the majority of HC focussing occurs in region from $0-8mm$ along the HC length with focussing effects saturating beyond $8mm$. These results mirror those of Hadjisolomou *et al.* reported in reference [12].

The spectra extracted from dose converted RCF for $< 0.5°$ divergent beams are shown in figure 3. Spectral peaks are observed for HC targets with proton numbers at least one order of magnitude greater than the same energy in the TNSA reference. The peak spectral energy increases with HC length with peaks located at $\sim 21MeV$, $\sim 25MeV$ and $\sim 30MeV$ for the $\sim 5mm$, $\sim 8mm$ and $\sim 12mm$ long HCs. Note that spectral peaks appear at similar energies for which the spatial profile showed a focussed beam. As HCs were of the same design, a similar synchronisation energy is expected, thus energy gain is proportional HC length as predicted. A narrower spectral peak is observed for the $\sim 12mm$ long HC compared to the $\sim 8mm$ suggesting the energy selection aspect of the HC is enhanced in longer HCs.

4 Particle Tracing Simulations

To explore the effect of helical coil (HC) length an exact replica of the $(700 + 125)\mu m$ diameter and $500\mu m$ pitch HC was constructed up to $12mm$ long in the particle tracing code *PTRACE* [18]. Experimental measurements of the EM pulse and TNSA seed beam reference parameters allowed exact replicas of the EM pulse propagating along the HC wire and the seed proton beam within the HC to be used as inputs.

The energy gain along the simulated HC is presented in figure 4 accompanied by divergence and spectral plots extracted at $5mm$, $8mm$ and $12mm$ along the HC. Corresponding experimental spectra from figure 3 are overplotted on simulation spectra as dotted lines. Tightly focussed beams are observed at $8mm$ and $12mm$ along the

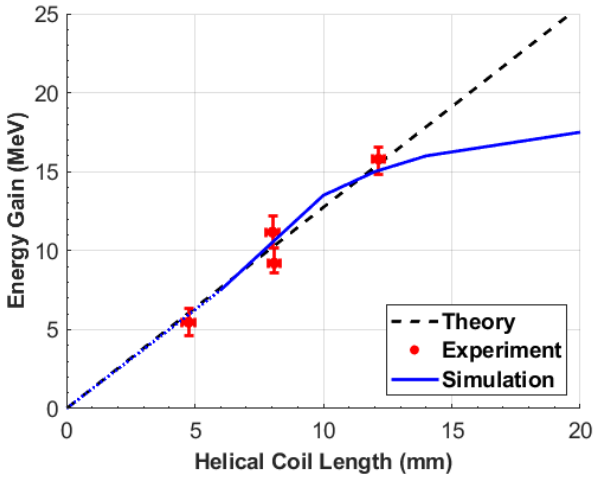

Figure 5: Energy gain as a function of helical coil (HC) length for experimental data (red dots) and particle tracing simulations (blue line). The $\sim 1.25 MeV/mm$ energy gain for the most effective HC length range, $0-12mm$, is extrapolated across the plot (black dashed line).

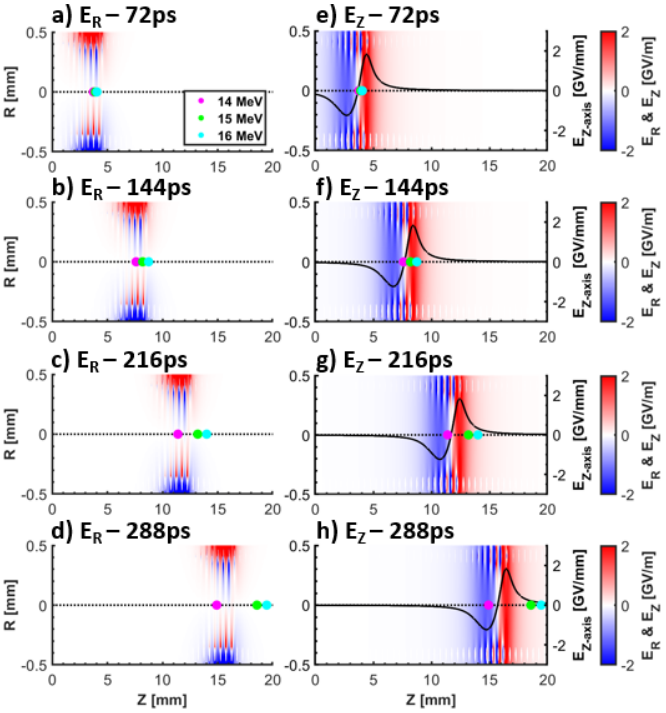

Figure 6: Radial focussing E_R **(a-d)** and longitudinal accelerating E_Z **(e-h)** electric fields inside a helical coil (HC) target. Field maps obtained in *PTRACE* simulations are shown for 72, 144, 216 & 288ps corresponding to peak EM pulse travel distances 4, 8, 12mm & 16mm along the HC axis Z. The longitudinal field profile along the HC axis E_{Z-axis} is over-plotted in panels (e-h). Also shown are the propagation of protons with original seed TNSA energies of $E_{sync} = 14,\ 15$ & $16 MeV$ as they are accelerated through the HC. At 12 & 16mm in (c, d, g & h) the protons originally with 15 & $16 MeV$ have outrun the strong radial and longitudinal fields by a few mm de-phasing with effective HC operation.

HC as seen in the experiment. The corresponding spectral peaks for $8mm$ and $12mm$ are located at $25 MeV$ and $30 MeV$ in good agreement with over-plotted experimental spectra. These spectral peak locations are retraced to a $15-16 MeV$ synchronisation energy from the seed beam, which is similar to estimated by equation 1. Due to the annular beam no obvious spectral peak is observed for the simulated $5mm$ long HC. Though considering the same $15-16 MeV$ synchronisation energy the corresponding output energy is $21 MeV$, the location of the spectral peak in the $5mm$ long HC experimental spectra. The synchronisation energy remains $15 MeV$ regardless of the HC length. A similar acceleration gradient is maintained over the entire $12mm$ long HC and $\sim 1.20 MeV/mm$, $\sim 1.25 MeV/mm$ and $\sim 1.25 MeV/mm$ calculated for $5mm$, $8mm$ and $12mm$ along the HC.

Figure 5 further shows that the energy gain saturates when HC length is increase beyond $12mm$. Similar observations have been made by Hadjisolomou *et al.* [12] and Ahmed *et al.* [13]. The interpretation offered was that the protons originally at the synchronisation energy are steadily accelerated until they outrun the strong annular EM field propagating along the HC axis and experience significantly reduced radial and longitudinal fields for the remainder of the HC length. De-phasing between the protons and the EM field is visualised in figure 6. At $4mm$ and $8mm$ along the HC axis protons remain within the region of strong radial and longitudinal EM fields. At $12mm$ along the HC axis the $15 MeV$ and $16 MeV$ protons are accelerated to $28.4 MeV$ and $30.0 MeV$, hence travel with a speed $1.4\times$ higher than the speed of the EM pulse along the HC axis. Hence a significant de-phasing of the accelerated protons from the EM field region. This begins to impact the HC effect, and becomes more pronounced at $16mm$, where the accelerated protons experience a weak EM field a few mm ahead of the peak field as shown in figure 6. Energy gain saturation is a concerning limitation of HC acceleration as efficient acceleration cannot be maintained simply by extending HC length.

5 Conclusion

Experimental data and supporting particle tracing simulations demonstrate that helical coil (HC) focussing and acceleration can be extended by increasing HC length. The majority of focusing is observed to occur in the first $8mm$ of the HC after which synchronised protons are observed in a $< 0.5°$ quasi-collimated beam. Efficient

acceleration is observed over the first $12mm$ of the HC before energy gain saturates. The reduced efficiency for extended HCs is due to the post-acceleration itself, causing originally synchronised protons to outrun and dephase from the strong annular electric field in the HC. Consequently, efficient energy gain is limited to $\sim 12mm$ for the $(700 + 125)\mu m$ diameter and $500\mu m$ pitch HCs studied, as highlighted by *PTRACE* simulations.

Acknowledgements

Authors acknowledge funding from EPSRC [EP/J002550/1-Career Acceleration Fellowship held by S.K., EP/L002221/1, EP/K022415/1, EP/J500094/1, and EP/I029206/1], SFB/TR18, GRK1203, EC-GA284464, and Invest Northern Ireland (POC-329). Authors greatly appreciate the hard work of the staff at the Central Laser Facility for making this research possible. Authors also acknowledge A. Schiavi for the use of the particle tracing code *PTRACE*.

References

[1] Macchi, A., Borghesi, M. & Passoni, M., *Ion acceleration by superintense laser-plasma interaction. Rev. Mod. Physics 85, 751 (2013).*

[2] Bulanov, S. V. *et al.*, *Oncological hadrontherapy with laser ion accelerators. Phys. Lett. A 299, 240 (2002).*

[3] Malka, V. *et al.*, *Practicality of proton therapy using compact laser systems. Med. Phys. 31, 1587 (2004).*

[4] Linz, U. & Alonso, J., *What will it take for laser driven proton accelerators to be applied to tumour therapy?. Phys. Rev. STAB 10, 094801 (2007).*

[5] Linz, U. & Alonso, J., *Laser-driven ion accelerators for tumor therapy revisited. Phys. Rev. Accel. Beams 19, 124802 (2016).*

[6] Quinn, K. *et al.*, *Laser-driven ultrafast field propagation on solid surfaces. Phys. Rev. Lett. 102, 194801 (2009).*

[7] Ahmed, H. *et al.*, *Investigations of ultrafast charge dynamics in laser-irradiated targets by a self probing technique employing laser driven protons. Nucl. Instrum. Methods A 829, 172 (2016).*

[8] Aktan, E. *et al.*, *Parametric study of a high amplitude electromagnetic pulse driven by an intense laser. Phys. Plasmas 26, 070701 (2019).*

[9] Kar, S. *et al.*, *Guided post-acceleration of laser-driven ions by a miniature modular structure. Nat. Commun. 7, 10792 (2016).*

[10] Kar, S. *et al.*, *Dynamic control of laser driven proton beams by exploiting self-generated, ultrashort electromagnetic pulses. Phys. Plasma 23, 055711 (2016)*

[11] Ahmed, H. *et al.*, *Efficient post-acceleration of protons in helical coil targets driven by sub-ps laser pulses. Sci. Rep 7, 10891 (2017).*

[12] Hadjisolomou, P. *et al.*, *Dynamics of guided post-acceleration of protons in a laser-driven travelling-field accelerator. Plasma Phys. Control. Fusion 62, 115023 (2020).*

[13] Ahmed, H. *et al.*, *Towards accelerator-quality, high energy proton beams employing laser-driven helical coils. Sci. Rep, manuscript accepted for publication (2021).*

[14] Breschi, E. *et al.*, *A new algorithm for spectral and spatial reconstruction of proton beams from dosimetric measurements. Nucl. Instrum. Methods A 522, 190–195 (2004).*

[15] Nürnberg, F. *et al.*, *Radiochromic film imaging spectroscopy of laser-accelerated proton beams. Rev. Sci. Instrum. 80, 033301 (2009).*

[16] Kriby, D. *et al.*, *Radiochromic film spectroscopy of laser accelerated proton beams using the FLUKA code and dosimetry traceable to primary standards. Laser Particle Beams 29, 231 (2011).*

[17] SRIM, *The Stopping and Range of Ions in Matter. (https://www.srim.org).*

[18] Schiavi, A., *Study of Laser Produced Plasmas by X-ray and Proton Radiography. Ph.D. thesis (Imperial College London, 2003).*

[19] Hadjisolomou, P., *Guiding and Post-Acceleration of TNSA Protons Employing Intense EM Pulse from the Laser-Foil Interaction. Ph.D. thesis (Queen's University Belfast, 2018).*